Reducing aeolian sand transport and beach erosion by using armour layer of coarse materials

Strypsteen, G. ; van Rijn, L.C.; Hoogland, M.D.; Rauwoens, P.; Fordeyn, J.; Hijma, M.; Lodder, Q.J.

DOI
10.1016/j.coastaleng.2021.103871

Publication date
2021

Document Version
Final published version

Published in
Coastal Engineering

Citation (APA)
Strypsteen, G., van Rijn, L. C., Hoogland, M. D., Rauwoens, P., Fordeyn, J., Hijma, M., & Lodder, Q. J. (2021). Reducing aeolian sand transport and beach erosion by using armour layer of coarse materials. *Coastal Engineering*, *166*, 1-15. Article 103871. https://doi.org/10.1016/j.coastaleng.2021.103871

Coastal Engineering 166 (2021) 103871

Contents lists available at ScienceDirect

Coastal Engineering

journal homepage: http://www.elsevier.com/locate/coastaleng

Reducing aeolian sand transport and beach erosion by using armour layer of coarse materials

G. Strypsteen [a,*], L.C. van Rijn [b], M.D. Hoogland [c], P. Rauwoens [a], J. Fordeyn [d], M.P. Hijma [e], Q.J. Lodder [f,g]

[a] Hydraulics and Geotechnics, Department of Civil Engineering, Bruges Campus, KU Leuven, Spoorwegstraat 12, 8200 Bruges, Belgium
[b] LVRS-Consultancy, Domineeswal 6, 8356D Blokzijl, the Netherlands
[c] Department of Physical Geography, Faculty of Geosciences, Utrecht University, the Netherlands
[d] Jan de Nul N.V., Tragel 60, 9308 Hofstade-Aalst, Belgium
[e] Department of Applied Geology and Geophysics, Deltares Research Institute, Daltonlaan 600, 3584 BK Utrecht, the Netherlands
[f] Rijkswaterstaat, Utrecht, the Netherlands
[g] Delft University of Technology, Faculty of Civil Engineering and Geosciences, P.O. Box 5048, 2600 GA Delft, the Netherlands

ARTICLE INFO

Keywords:
Beach armouring
Roughness of bed forms
Modified bagnold-transport equation
Aeolian transport

ABSTRACT

A man-made dune-beach-spit system at the south-east side of the island of Texel (Prins Hendrik site) has been built in 2018–2019 to strengthen the traditional dike. The core of the dune-beach-spit system consists of medium fine sand with a d_{50} of 0.25–0.3 mm. The beach is covered with an armour (protection) layer of coarse materials with relatively large gravel and shell fractions to reduce wind erosion and thus maintenance costs. In the design phase of the project the aeolian sand transport model of Bagnold was used to estimate the long-term erosion losses of sand at the new dune-beach system. This transport model was validated in the design phase by using detailed sand transport and bed roughness measurements at a nearby site called The Hors. This site is a wide natural beach plain of sand (d_{50} = 0.23 mm), where 147 high-quality datasets have been collected using a wind mast equipped with 5 cup anemometers and various sand traps. It is shown that the measured sand transport rates at the Hors can be reasonably well represented by the modified Bagnold-equation for dry sand. After completion of the new dune-beach system, a field experiment was performed at the Prins Hendrik site to verify the sediment transport predictions and erosion loss of sand. Data from two permanent wind masts and one short, mobile wind mast were used to derive the effective roughness of (stationary) bed forms. Sand transport rates were measured at various locations using a new trap sampler. The measured sediment transport in the armoured beach zone can be reasonably well represented by the Bagnold-equation using a multi-fraction approach with hiding-exposure coefficient. The predicted transport rates have been used to estimate the annual loss of sand from the Prins-Hendrik site.

1. Introduction

Very few detailed field studies on selective aeolian transport processes in conditions with sand, gravel, shells (armouring) and moving and stationary bed forms are available (Carter, 1976; Carter and Rihan, 1978; Tan et al., 2013; Hoonhout and de Vries, 2017). Yet, these studies are necessary for the prediction and management of beach-dune responses to wind forces on short to long-term time scales.

A practical example is the design and construction of a new dune-beach-spit system at the island of Texel, a barrier island along the Dutch Wadden Sea of The Netherlands. This new system was designed and built (2017–2019) in front of a traditional dike covered with asphalt and grass (Prins Hendrik dike/site; PH-dike/site) which was unsafe for future protection of the low-lying hinterland (polder) against storm floods. Major issues in the design phase of this new dune-beach-spit system were the high long-term maintenance costs related to sand losses due to wind erosion during storms and no natural resupply of sand. Available field measurements at a nearby site (The Hors) were used to validate the aeolian transport model applied (modified Bagnold equation) for dry sand conditions. This detailed field dataset of shear

* Corresponding author.
E-mail addresses: glenn.strypsteen@kuleuven.be (G. Strypsteen), info@leovanrijn-sediment.com (L.C. van Rijn), m.d.hoogland@students.uu.nl (M.D. Hoogland), pieter.rauwoens@kuleuven.be (P. Rauwoens), jan.fordeyn@jandenul.com (J. Fordeyn), marc.hijma@deltares.nl (M.P. Hijma), quirijn.lodder@rws.nl (Q.J. Lodder).

https://doi.org/10.1016/j.coastaleng.2021.103871
Received 10 September 2020; Received in revised form 7 December 2020; Accepted 19 February 2021
Available online 4 March 2021

velocities, bed roughness values and sand transport rates was collected in 2000, and has never been published before. As validation for armoured beach conditions was not possible due to lack of field data, it was found difficult to estimate future sand losses at the PH-site with a coarse armour layer of gravel and shells using existing transport equations. After completion of the new dune-beach system in 2019, an extensive field experiment was initiated in Spring (2020) to study the wind erosion processes at the artificial beach and spit covered with a coarse armour layer with the aim to verify and improve the existing design tools for aeolian transport and beach armouring.

Until today, it is still difficult to adequately measure saltation and creep transport, especially in the field due to the high temporal and spatial unsteadiness of the wind flow and scour around the deployed instruments such as sand traps, impact detectors, and optical sensors. Mechanical trap-type instruments are still the most reliable for aeolian sand transport measurements. However, these instruments are intrusive and have problems in measuring the sand transport close to the sand surface resulting in a trap efficiency (ratio of measured and true transport) smaller or larger than 1, depending on the design of the trap, wind speed, particle diameter, and sampling time (Goossens and Offer, 2000).

The measurement of aeolian sand transport is even more complicated in conditions with a coarse armour layer. Aeolian sand transport is reduced when the surface is covered with high quantities of gravels, shells and shell clusters, which are known as aeolian shell-gravel pavements (Carter, 1976; Carter and Rihan, 1978). In these conditions, the supply of sediment is limited by the presence of non-erodible roughness elements within the surface sediments. As erosion proceeds, the larger, non-erodible fraction becomes more exposed and remains at the surface as a deflation lag deposit, limiting the transport to almost zero at given wind-induced stress. Initially, the sand transport may increase slightly due to generation of additional turbulence and local velocity accelerations around the immobile coarse grains and shells. Eventually, the sand transport reduces significantly as the shear stresses exerted on the smaller grains between the larger coarse grains are significantly reduced to below the threshold shear stress for entrainment. A higher wind-induced stress is required for further erosion of the smaller grains from beneath the coarser grains. Lag deposit surfaces can be observed at agricultural fields (Chepil and Woodruff, 1963; Lyles et al., 1974) and at nourished beach sites (De Vries et al., 2014; Hoonhout and de Vries, 2017, 2019).

Some studies on the effect of non-erodible coarse grains on aeolian transport have been done in the past. The effect of relatively large, non-erodible roughness elements on a surface of erodible particles was studied in a wind tunnel by Gilette and Stockton (1989) and by Nickling and McKenna (1995). Their test results indicate the gradual development of a deflation lag. Initially, there is an increase in sediment flux above the rippled sand bed because of increased erosion around the emerging roughness elements. As the roughness elements are more exposed (higher emergence), the sediment flux decreases rapidly, tending towards zero.

Tan et al. (2013) studied the change in sand transport from a pure sand bed to a bed covered with gravel (20–55 mm) using a mobile wind tunnel operated in the Gobi Desert in China. The sand transport was reduced by about 20%–50% for increasing gravel coverage from 10% up to 70% due to the decrease of the wind velocities in the lowest layer of 50–100 mm above the surface. Similar findings are given by Gillies et al. (2006). They found that wind-blown sand transport is substantially reduced (up to 90%) if numerous roughness elements are present on a sand surface.

Van Der Wal (1998) studied the effect of shells (coverage up to 30%) on the wind-induced transport rate of sand taken from 5 different sites with d_{50} in the range of 0.21–0.35 mm. The sand transport rate at the end of a long tray in a wind tunnel was reduced by about 30% for a shell percentage of 7% and by about 70% for a shell percentage of 25%. Shell pavements were formed during the wind tunnel experiments. This was also observed by McKenna et al. (2012). Shells (up to 30% in a wind tunnel) showed spatial organization resulting in shell clusters of partly interlocking shells of different sizes. The threshold wind velocity and shear velocity were found to increase up to 45% for a cover of maximum 43% and erosion was reduced by a factor of 5–10. Crushed shells are found to be less effective than small/large shells.

Some field studies on beach armouring processes have been performed earlier, but quantitative results of aeolian transport rates are almost absent. Beach armouring was observed at two nourished beach sites south of The Hague, The Netherlands (De Vries et al., 2014; Hoonhout and de Vries, 2017, 2019). Sand transport processes were studied in December 2010 at Vlugtenburg beach after nourishment with sand containing a relatively large amount of shell fragments. Due to sorting processes over time, the shell fragments form lag deposits at the upper beach, but the lag deposits were continuously reworked in the intertidal zone resulting in patches of finer and coarser sediments. Lag deposits were also formed at the Sand Motor beach south of The Hague, which is a large-scale artificial beach plain (nourishment 2011; $d_{50} = 0.35$ mm; 5% coarse > 2 mm) with surface level at $+5$ m above mean sea level (Hoonhout and de Vries, 2017, 2019). Over time, the percentage of coarse materials of the top layer gradually increased to about 20% due to winnowing of finer sand blown away in downdrift directions. This process resulted in significant limitations of the sand transport rates of finer sediment.

It is realized that these earlier research results in wind tunnels and at field sites are somewhat diverse, but all information points to a significant reduction of the sand transport rate for increasing coverage and roughness height of coarse materials. However, a generally accepted method to include these effects is not yet available and thus we have to rely on partly empirical methods to be able to make predictions for engineering designs.

The two most basic research questions related to the topics discussed above are:

- what is the bed roughness of (armoured) beaches with bed forms and what is the most relevant driving parameter for wind-driven transport (overall shear velocity or grain-related shear velocity)?
- what is the effect of coarse materials > 2 mm (including shells) on aeolian transport and beach armouring and what is the annual erosion loss of sand at an armoured beach site without supply of sediment at the upwind boundary?

These research questions are extensively addressed in this paper based on detailed sediment transport measurements. High-quality data have been collected at two beach sites at the island of Texel and are presented in tabulated form in this paper to extend the international database. The sites and instruments are described in Section 2 and 3. Transport prediction methods are presented in Section 4. Bed roughness values derived from measured wind velocity profiles are discussed in Section 5. Results of measured and predicted transport rates for validation of the sand transport model used are given in Section 6. Finally, sand transport predictions based on annual wind velocity data are used to estimate the annual erosion losses of sand at the artificial PH-site covered with an armour layer.

2. Description of the study sites

2.1. Beach plain The Hors

Field experiments on aeolian sediment transport were conducted on The Hors (Hijma and Lodder, 2001), The Netherlands in summer and autumn of 2000. The Hors is a large flat sand plain (2 km wide; 4 km long) between the sea and the foredune on the south side of the barrier island of Texel in the Dutch Wadden Sea (Fig. 1). The beach plain has been growing since the Middle Ages and consists of sand with an average d_{50} of about 0.23 mm. Small, barchan-like mega-ripples of about 0.05 m high and several meters long are migrating along the beach surface

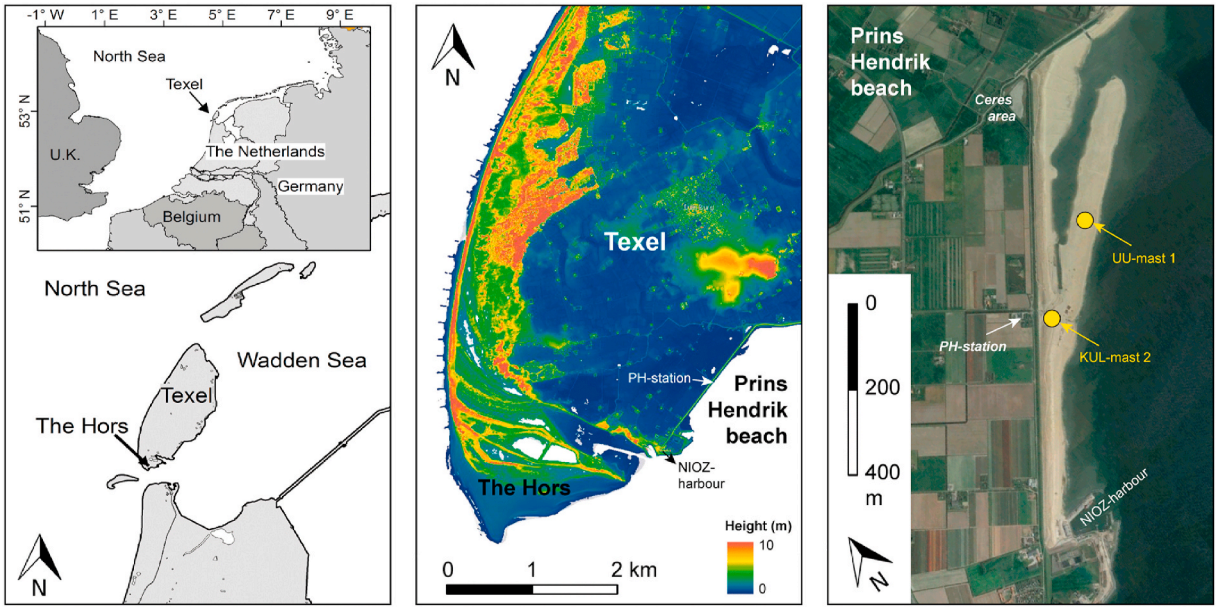

Fig. 1. Location of the study areas.

during windy conditions. The field experiments were done at the landward side of the beach plain, more than 1 km away from the shoreline.

2.2. Dune-beach-spit Prins Hendrik (PH)

Field measurements were conducted (12 March to April 21, 2020) on the new man-made sand dune, beach and oblique spit at the south-east side of the island of Texel (Fig. 1). The man-made Prins Hendrik dune-beach-spit system consists of sediment dredged from a location in The North Sea. The core of this system consists of medium fine sand with d_{50} of 0.25–0.3 mm. The beach is covered with a protection layer (about 0.3 m thick) of coarse sand, gravel and shells to reduce the wind erosion and thus the maintenance costs, as there is no supply of sand across the boundaries of the site. This coarse layer was placed on the beach and spread out by shovels. During and after construction on a time scale of 6–12 months, the finer sand grains were gradually removed by wind erosion leaving a layer of coarse sand, gravel and shells (armour layer). The sediment characteristics of surface samples of the top layer of 10–20 mm from the period 23 October to December 1, 2018 after construction are: $d_{50} \cong$ 0.5–1 mm at the south part of the dry beach between NIOZ-harbor and PH-pumping station; $d_{50} \cong$ 0.6–2 mm at the north part with the spit and $d_{90} \cong$ 2–5 mm at both parts. The largest gravel size is about 10 mm. The percentage of sediment with grain sizes $>$ 2 mm varies in the range of 15% to almost 100%. These particle size ranges are representative for the conditions during the field work in Spring (2020).

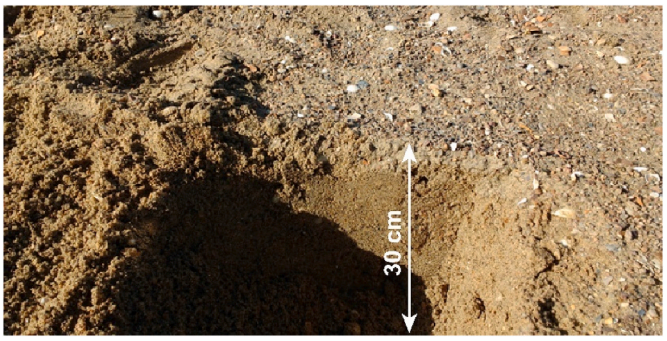

Fig. 2. Vertical structure and composition of top layer with armour layer and deeper coarse sand layer, PH-beach site, Texel.

An impression of the thickness of the armour layer can be observed from Fig. 2, showing a thin upper layer with coarse materials (thickness of 5–10 mm) and the subsoil with much less coarse materials.

At many places, the PH-beach is covered with 3D undulating types of bed forms with heights in the range of 0.05–0.25 m and lengths of 1–3 m (Fig. 3B). These bed forms are immobile during wind conditions up to 15 m/s due to the presence of a coarse armour layer of gravels and shells.

Two wind masts (UU-mast 1 and KUL-mast 2; Figs. 1 and 3) were placed at the PH-site. Most sand transport measurements have been done near KUL-mast 2 which is positioned in the cross-section near PH pumping station (Fig. 1). At this location near mast 2, the cross-shore profile consists of:

- Wet intertidal beach of 5–30 m wide with coarse sand andshell/gravel clusters;
- Dry beach of 100–120 m wide separated from the wet beach by a scarp line ($\cong$ 0.5 m high). The dry beach is at 2.5 m above mean sea level and covered with a coarse armour layer of sand, gravel and shells;
- Dune foot zone of finer sandy materials protected by grass plants and short wind breaking brushwood fences made of long twigs ($\cong$ 1 m high).

3. Methodology

3.1. Instrumentation at beach plain The Hors

Wind velocities were measured using five cup anemometers positioned at elevations of 0.20, 0.35, 0.85, 1.35 and 1.95 m above the sand surface (Fig. 3A). The wind velocity distribution is described by:

$$U_z = \frac{u_*}{\kappa} \cdot ln\left(\frac{z}{z_0}\right) \quad (1)$$

Where U_z = wind speed at z above surface, κ = von Karman's constant (= 0.4), and z_0 = roughness length of surface ($z_o = k_s/30$, k_s = equivalent roughness height; Nikuradse 1933). Log-linear regression is used to obtain the optimal parameter set of u_* and z_0 (Bauer et al., 1992). It is realized that the validity of a logarithmic profile may be questionable for field sites with more wind gustiness as opposed to laboratory conditions. However, the regression coefficients of the measured velocity profiles at

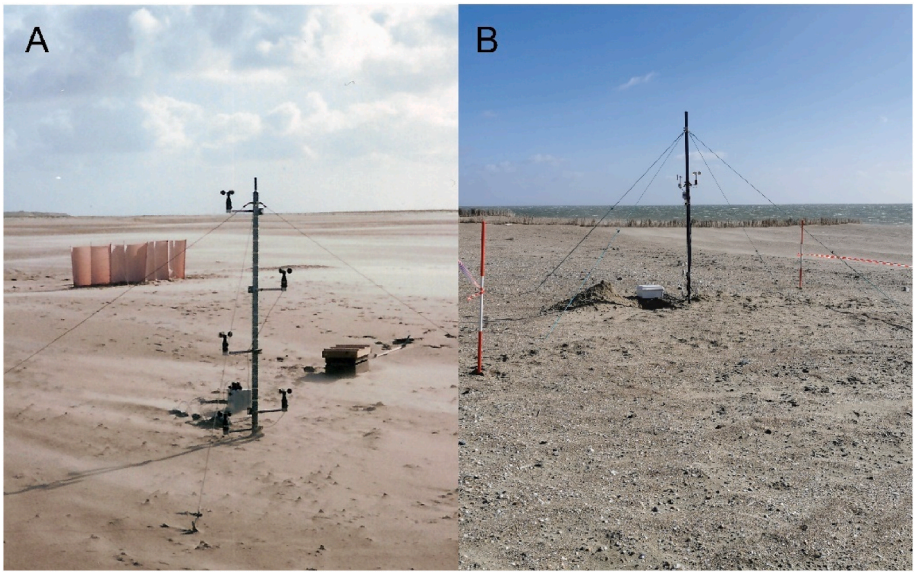

Fig. 3. Wind mast at The Hors beach (A) and PH-beach with bed undulations (B).

both masts are high for all data ($R^2 > 0.98$) confirming the validity of logarithmic velocity profiles.

Three different sand traps (Fig. 4) have been used: Bagnold trap (Bagnold, 1938), Sarre trap which is a modification of the Leatherman trap (Sarre, 1988) and a slot-type creep trap from University of Utrecht. The slot-type trap is a box with a slot-opening of 10 mm and 50 mm wide (Fig. 4C). All trap openings are placed into the direction of the wind at about 1 m from the wind mast; each run was 10–20 min. Detailed descriptions are given by Hijma and Lodder (2001).

3.2. Instrumentation at Prins Hendrik site

Wind velocities were measured at 2 long masts with 4–5 wind cup meters on each mast (Fig. 1). In addition, wind velocities were also

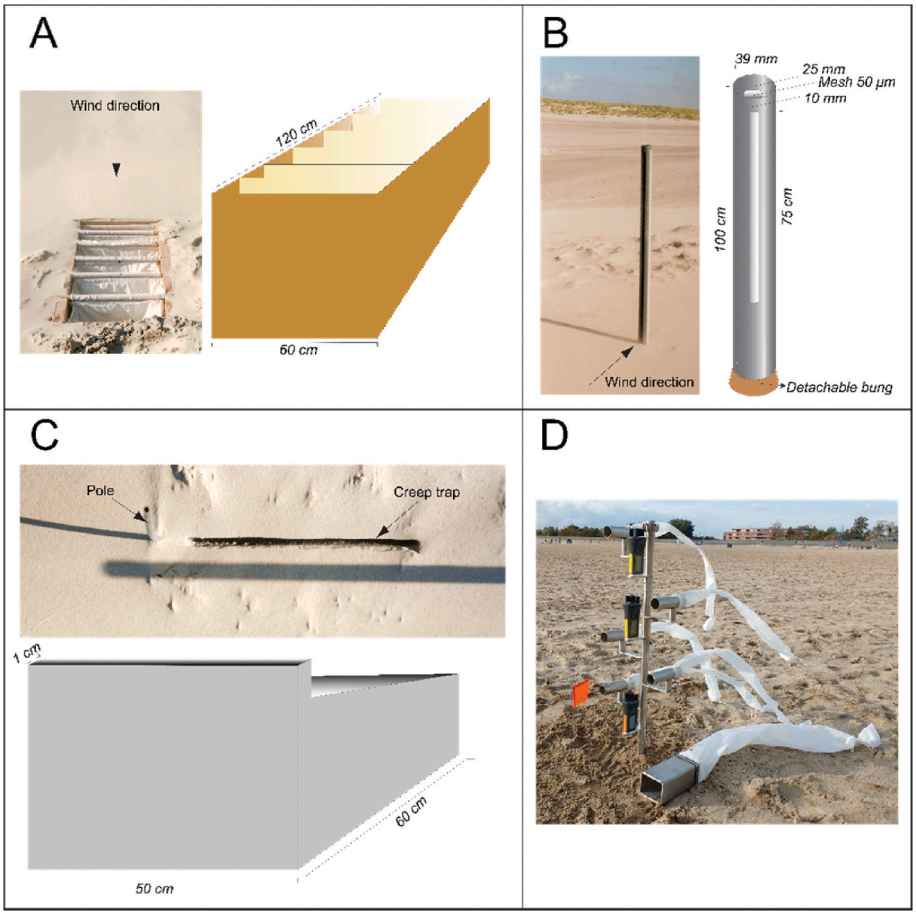

Fig. 4. A) The Bagnold trap, B) The Sarre trap, C) The Creep trap and D) LVRS-trap.

measured at many other locations using a short, movable mast with three wind cup meters (Fig. 5D).

Sand transport at the PH-site was measured using the new LVRS-trap (Fig. 4D) consisting of a short mast with three wind speed meters (JDC-eole; inaccuracy ± 3%) and four circular tubes (36 mm diameter) for trapping of saltating particles. A separate bed load trap (height 71 mm; width 93 mm) is used. All traps have nylon bags with 70 μm mesh. The regression coefficients of the velocity profiles with three data points are slightly smaller ($R^2 > 0.95$) than those of the 2 long masts with 4 velocity data resulting in slightly lower accuracy of the shear velocities derived from the short mast data. It is noted that the wind velocities of the short mast (and not the bed shear velocities) are used to drive the sand transport model proposed by van Rijn and Strypsteen (2020). This model only requires the specification of one velocity at a given height above the surface, and the bed roughness is fully predicted (see Section 4). The LVRS-sand trap is similar to the high-efficiency Sherman streamer trap (SST; Sherman et al., 2014) as scour at the corners of the mouth is absent and no sand is accumulating in front of the sampler. The sampling unit can be setup quickly (minutes) to obtain measurements at many locations or many samplings at a fixed location. Based on experience of many measurements, the transport of sand in the layer 0–71 mm measured by the bed load trap is mostly about 70% of the total transport for high wind speeds to about 100% for low wind speeds. The transport in the upper layers is derived by interpolation from the measured fluxes defined in the center points of the tube-type traps (Ellis et al., 2009). Small interpolation errors may occur in determining the transport of sand in the upper layers. The overall error of the total transport is estimated to be less than 15%.

4. Aeolian transport models

4.1. Single fraction method

One of the most cited benchmark equations, concerning aeolian transport calculations, is that from Bagnold (1937). The equation of Bagnold is only valid for shear velocities higher than the threshold shear velocity, and can be described by:

$$Q_s = C_B \cdot \sqrt{\frac{d_{50}}{D}} \cdot \frac{\rho_{air}}{g} \cdot u_*^3 \tag{2}$$

Where D = reference grain diameter of 0.25 mm, d_{50} = median grain diameter of the sand, and C_B = constant of 1.5 for nearly uniform sand, 1.8 for naturally graded sands. ρ_{air} = density of air (taken as 1.2 kg/m^3), g = gravity constant (taken as 9.81 m/s^2) and u_* = shear velocity.

Bagnold (1941) also formulated the bed-shear velocity for threshold conditions as:

$$u_{*,th,B} = \alpha_{th} \cdot \sqrt{\left[\left(\frac{\rho_s}{\rho_{air}} - 1\right) \cdot g \cdot d_{50}\right]} \tag{3}$$

where α_{th} = empirical constant; herein taken as 0.1 based on more recent data of Shao and Lu (2000) and Han et al. (2011). Van Rijn and Strypsteen (2020) have recently proposed a modified version of the Bagnold-model. Two modifications are included: 1) the use of a threshold shear velocity and 2) the use of the dynamic grain-related shear velocity instead of the overall shear velocity. The modified version of the Bagnold-equation for aeolian transport (van Rijn and Strypsteen, 2020) reads as:

$$q_{s,eq} = \alpha_B \cdot \alpha_{ad} \cdot \alpha_{cf} \cdot \sqrt{\frac{d_{50}}{D}} \cdot \frac{\rho_{air}}{g} \cdot \left(u_{*,grain}^3 - u_{*,th}^3\right) \tag{4}$$

$$u_{*,th} = \alpha_w \cdot u_{*,th,B} \tag{5}$$

$$u_{*,grain} = \kappa \cdot \frac{U_w}{ln\left(\frac{30 \cdot z_w}{k_{s,grain}}\right)} \tag{6}$$

with: $q_{s,eq}$ = mass sand flux at equilibrium conditions (kg/m/s); d_{50} = particle size (m); ρ_s = sediment density (2650 kg/m^3); $u_{*,grain}$ = shear velocity related to the static and dynamic grains (m/s); $u_{*,th}$ = threshold shear velocity (m/s); $k_{s,grain}$ = equivalent roughness of Nikuradse (m) related to grains; U_w = wind velocity at z_w above sand surface (m/s); κ = constant of Von Karman (= 0.4); α_w = moisture coefficient (equal to 1 for dry sand); α_{cf} = reduction coefficient related to the presence of coarse fraction; α_{ad} = adjustment coefficient related to fetch (maximum 1 for a long fetch; van Rijn and Strypsteen, 2020).

The driving parameter of the modified Bagnold equation is the grain-related shear velocity ($u_{*,grain}$). This parameter is given by the following expressions (van Rijn and Strypsteen, 2020):

$$k_{s,grain} = k_{s,grain,stat} + k_{s,grain,dyn} = d_{90} + \alpha_1 \cdot \gamma_r \cdot d_{50} \cdot T^{\alpha_2} \tag{7}$$

$$T = \frac{\left[u_{*,grain,stat}\right]^2 - \left[u_{*,th,B}\right]^2}{\left(u_{*,th,B}\right)^2} \geq 0 \tag{8}$$

$$u_{*,grain,stat} = \kappa \cdot \frac{U_w}{ln\left(\frac{30 \cdot z_w}{d_{90}}\right)} \tag{9}$$

where: T = transport parameter (−); $u_{*,grain,\ stat}$ = shear velocity related to static grains (based on Equation (6) with $k_{s,grain,\ stat}$); $u_{*,th,B}$ = threshold shear velocity of Bagnold; $k_{s,grain,\ stat}$ = roughness height due to static grains taken as d_{90} (m); $k_{s,grain,dyn}$ = bed roughness height related to the dynamic moving grains, $k_{s,grain}$ = bed roughness height due to static and dynamic grains (m); d_{90} = grain diameter; $\gamma_r = 1 + 1/T$ = ripple enhancement coefficient; $\alpha_1 = 15$ and $\alpha_2 = 1$.

The coefficients α_1 and α_2 are empirical coefficients which have been calibrated by Van Rijn and Strypsteen (2020) and are also used in the present study as known values. Similarly, the α_w-coefficient for moist sand has been determined by Van Rijn and Strypsteen (2020) and is also used in this study. The Bagnold-coefficient (α_B) is set to 2 as proposed by Van Rijn and Strypsteen (2020) giving the best agreement between measured and predicted values for various datasets.

The α_{ad}-coefficient can be used to include conditions with a short fetch length ($\alpha_{ad} = 1$ for a long fetch > 100 m), as discussed in Section 7. The fetch lengths at both sites of this study are long > 500 m for the dominant wind directions ($\alpha_{ad} = 1$).

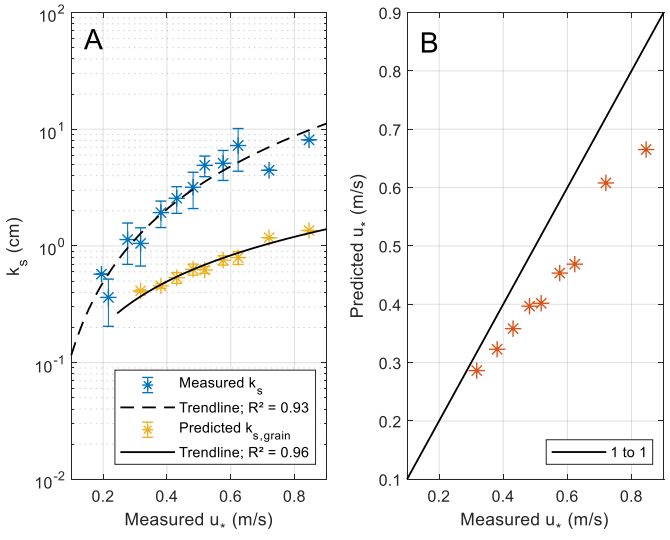

Fig. 5. A) Change of measured and predicted roughness length at The Hors, B) Comparison between measured shear velocity and predicted grain-shear velocity at The Hors.

The α_{cf}-coefficient represents the effect of coarse immobile materials (gravel, shells) on the sand transport processes. The two main effects are: i) coarse materials cover a certain area of the bed which is not available for sand particle erosion and ii) sand particles in the direct vicinity of coarse materials are less exposed to the wind forces (hiding effect). Observations in wind tunnels and field conditions show that shells of different sizes tend to interlock and form clusters shielding the underlying sand surface against erosion (spatial organization; Mckenna et al., 2012; Strypsteen, 2019). Van Rijn and Strypsteen (2020) have shown that the reduction effects can be simply represented by a reduction factor acting on the transport rate: $\alpha_{cf} = (1\text{-}2p_{cf}/100)^2$ and p_{cf} = percentage of coarse materials (%). This empirical relationship is used in the present study.

The α_w, α_{cf}, α_{ad}-coefficients are necessary to deal with moist sand, course sediment (gravel and shells) and short fetch lengths. It is noted that the default values of all model coefficients are used in this study (based on earlier work of Van Rijn and Strypsteen, 2020); no additional calibration has been done.

4.2. Multi-fraction method

A more scientific method to take the effect of the coarse fraction and subsequent armouring into account is the multi-fraction method which is most suitable for conditions with a relatively wide size grading ($d_{90}/d_{10} > 5$) based on the detailed physical work and experiments of Egiazaroff (1965). This method reads as:

$$q_{s,eq} = \alpha_B \cdot \alpha_{ad} \cdot \alpha_{cf} \cdot \frac{\rho_{air}}{g} \cdot \sum_{i=1}^{N} \left[f_i \cdot \sqrt{\frac{d_i}{D}} \cdot \left[u_{*,grain}^3 - \left(\zeta_i \cdot u_{*,th,i} \right)^3 \right] \right] \quad (10)$$

with: N = number of fractions, d_i = mean particle size of fraction i, f_i = fraction value (< 1; $\sum f_i = 1$), ζ_i = hiding-exposure factor (finer particles are shielded by larger particles and are more difficult to erode), $u_{*,th,i}$ = threshold shear velocity of fraction i. The α_{th}-coefficient of the threshold equation is set to $\alpha_{th} = 0.1$ for each fraction (assumed to be uniform). The hiding-exposure factor (minimum value = 1) is tentatively expressed by (Van Rijn, 2007):

$$\zeta_i = \left(\frac{d_{50}}{d_i} \right)^n \quad (11)$$

with: n = 0.5 to 1. The application of Equation (11) is necessary to obtain realistic transport rates. Just summing of the fraction contributions will lead to overestimation of the transport rates. The effect of Equation (11) is similar to the artificial weighting function used by Hoonhout and Vries (2016).

If shells are present, it is assumed that each fraction is affected in the same way. Sediment particles under the shells do not participate in the transport process, which is taken into account by the percentage of shells (p_{shell}) per unit mass. Particles in the lee of the shells experience lower wind speeds and are thus less mobile. This effect is taken into account by a reduction coefficient (α_{cf}) acting on the transport rate (van Rijn and Strypsteen, 2020).

5. Bedform roughness and grain-related roughness

5.1. Bed forms and bed roughness

Most aeolian transport equations are based on the overall shear velocity, which is an indirect parameter derived from measured wind velocity profiles. If wind velocity profiles are absent, the bed-shear velocity has to be predicted requiring information of the local bed roughness (k_s or z_o). The beach surface is generally covered with small bed forms (ripples) during low to moderate wind conditions, but the ripples are smoothed out by storm winds (> 15–20 m/s). Knowledge of the bed roughness under varying wind conditions is of utmost importance for engineering computations. Pelletier and Field (2016) and Field and Pelletier (2018) studied the roughness related to ripples and saltation-related grains. Their results show that the form-related roughness is much larger than the grain roughness effects. Van Rijn and Strypsteen (2020) have proposed to use the dynamic grain-related shear velocity as the driving parameter rather than the overall shear velocity for transport computations. The data of both sites on Texel are used to validate this approach.

5.2. Measurements and analysis results for beach plain The Hors

The bed-shear velocities and bed roughness values derived from the field data are shown in Tables 1 and 2 (Appendix A). Fig. 5A shows the measured roughness as function of the shear velocity.

The measured roughness increases from 0.1 to 10 cm and the predicted roughness from 0.2 to 1.5 cm for shear velocities increasing from 0.2 to 0.85 m/s. As the overall roughness depends on both the geometry of the bed (ripples) and the saltating sand grains, the increase of the overall roughness can be explained by the growing bed form dimensions from ripples to larger barchan-like mega-ripples (50 mm high) during increasing wind velocity. The measured roughness is about equal to 1 to 2 times the height of the ripples. The predicted roughness of Fig. 5A represents the (static and dynamic) grain-related roughness based on the roughness predictor (Equation (7)) which is much smaller than the overall roughness derived from the measured velocity profiles. Fig. 5B shows the comparison between measured shear velocity and predicted grain-related shear velocity based on the roughness predictor. The predicted shear velocity is the grain-related shear velocity and is about 20% smaller than the total shear velocity derived from the velocity profiles. This was also found by Van Rijn and Strypsteen (2020). It is noted that the grain-related shear velocity is used to predict the sand transport rate (Equation (4)).

5.3. Measurements and analysis results for Prins-Hendrik beach

The beach surface near both masts (Fig. 1) is covered with almost immobile three-dimensional features which are herein typified as surface undulations because of the smooth, wave-type appearance (Fig. 3B). The undulations are 0.1–0.25 m high near mast 1 and 0.05–0.15 m high near mast 2. The length scale at both locations is about 1–3 m. The top layer of these undulations consists of coarse sand, gravel and shells. Five minor storm events on 12, 21, 27, 29 March and April 13, 2020 have been selected for analysis of velocity profiles.

Detailed measurements with the short mast were done on 27 March with winds of 10–14 m/s from northeast almost parallel to the beach. Wind velocities were measured at 10 locations (close to mast 2) with spacings of 20 m in a transect parallel to the wind (and beach). Sand transport was absent due to the presence of the armour layer. Fig. 6 shows the wind data of mast 2 over a period of 480 min and the wind data of the short mast over 140–180 min. The short mast wind data are 1 min-averaged wind velocities at 0.3, 0.5 and 1.25 m, repeated at least 5 times at each location. The overall agreement between the wind velocity data of mast 2 and the short mast is good. The short mast velocities are slightly more variable as this mast was placed at different locations within the bedform field. Logarithmic velocity profiles were fitted to the data of both masts to derive the shear velocity and the bed roughness. The R^2-values were > 0.95 for the short mast and > 0.98 for the long mast 2. The bed roughness values are in the range of 20–50 mm for mast 2 and in the range of 70–150 mm for mast 1, see Figs. 6 and 7. These values are smaller than the bed form heights which is typical for relatively long and wavy-type bed forms (van Rijn and Strypsteen, 2020).

Fig. 7 shows the measured bed shear velocity at mast 1 and 2. The shear velocity at the more exposed mast 1 (Fig. 1) is slightly higher. Also shown are the predicted grain shear velocity at mast 1 and 2 based on the method of van Rijn and Strypsteen (2020). The threshold shear velocities for particles of 0.3 and 3 mm are indicated as dashed lines,

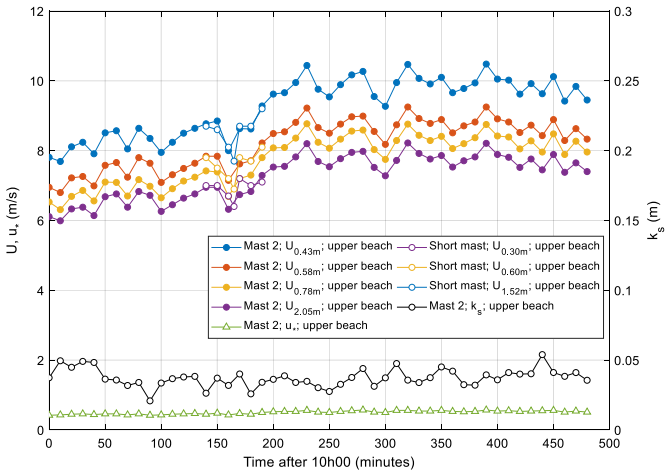

Fig. 6. Measured wind velocities, shear velocities and bed roughness at upper beach at mast 2 and at the short mast, 27 March; wind from north and north-east.

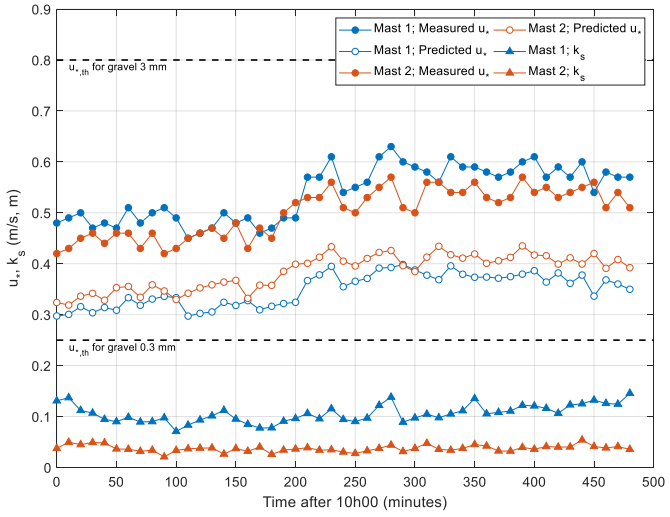

Fig. 7. Measured shear velocity and predicted dynamic grain shear velocity at both masts 1 and 2 as function of time, March 27, 2020; wind from north and north-east.

expressing that particles of 0.3 mm are mobile, but coarse particles of 3 mm are immobile. The predicted grain shear velocities are smaller (≅ 30%) than the measured overall shear velocity. The latter is mainly determined by the form roughness of the surface undulations. The grain shear velocity represents the roughness of the stationary coarse grains of the armour layer. It is noted that the use of the overall shear velocity in transport equations will lead to higher transport rates and may be the reason for the overprediction of some equations (de Vries et al., 2014; Sherman et al., 1998, 2013).

The short mast was also used to measure velocity profiles at flatter spots close to the crests of the undulations. The bed roughness derived from the data is the range of 1–2 mm, which is of the scale of the coarse grains of the armour layer. Thus, the wind flow is dominated by both the large-scale roughness structure (dimensions of the bed undulations) as well as the grain size of the of coarse gravel armour layer and the many shells resting on the armour layer.

6. Measured and predicted sand transport

6.1. Sand transport at beach plain The Hors

A total of 147 transport rates were measured: 65 with Bagnold trap, 42 with Sarre trap, and 40 with the creep trap. The transport rates have been binned in shear velocity intervals of 0.05 m/s (velocity intervals of about 1 m/s) and are shown in Fig. 8A and Table 3 (Appendix A). Comparison of simultaneous measurements showed that the Bagnold trap systematically produced higher values of the order of 30%–50% than the Sarre-trap in line with the findings of Al Khalaf (1986; In: Sherman, 1990 and Sherman and Hotta, 1990). Therefore, the Bagnold-trap values were corrected by a factor of 1.4. The creep trap results are systematically lower, which is logic as the creep trap only measures the transport by rolling and gliding particles. Bagnold (1941, 1954) assumes that the ratio of creep and saltation transport has a constant value of 1/3, independent of the wind velocity. The results given in Fig. 8A and B shows that the creep quotient is not constant as proposed by Bagnold (1941), but instead depends on shear velocity in agreement with the theoretical analysis of Wang and Zheng (2004).

The measured sand transport rates at The Hors at higher shear velocity values > 0.3 m/s are in reasonable agreement with the predicted values of the modified Bagnold-method (Equation (4)) with standard coefficients. The measured values at relatively small shear velocities (0.2–0.3 m/s) are systematically underpredicted. The power relationship between transport and shear velocity is found to be reasonably valid over the full range of conditions. Summarizing, it is concluded that the modified Bagnold-equation can be used with confidence (validation result) for predicting the transport of dry sand in the range of 0.2–0.25 mm.

6.2. Sand transport at Prins Hendrik beach

Transport measurements have been done at the wet beach, dry beach, dune foot, dune front and dune crest. All transport data are shown in Table 4 (Appendix A) and in Fig. 9. A detailed description of the beach and wind conditions is given by Van Rijn (2020).

6.2.1. Wet intertidal beach

Measurements were done at 5–10 m from the water line near mast 2 with moisture levels of 4%–12% during minor storms from SW (parallel to beach) on march 12, 2020 and from NNE (parallel to beach) on March

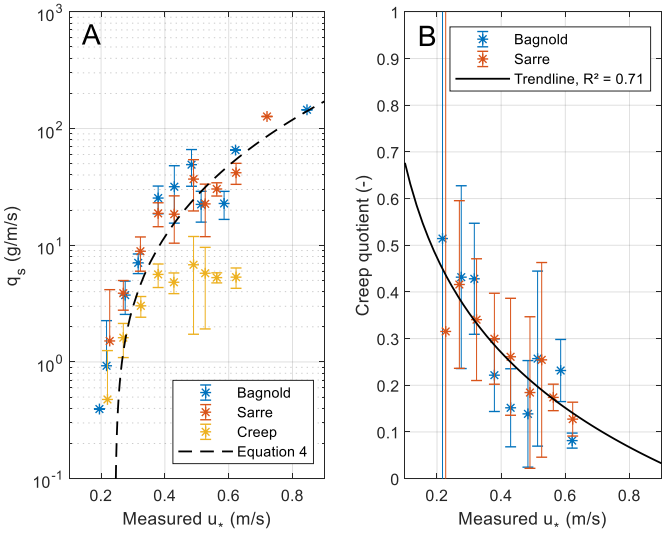

Fig. 8. A) Binned transport rates with measured shear velocities on The Hors and predicted transport rates, B) Creep quotient with measured shear velocities on The Hors.

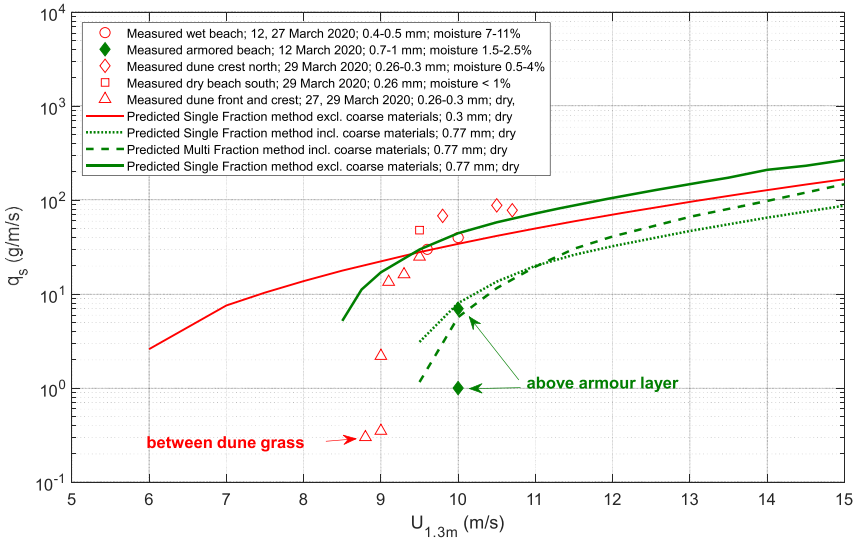

Fig. 9. Measured and predicted sediment transport values, PH-site, Texel.

27, 2020. Moisture contents were measured by taking samples for drying and weighing. Sand transport was intensive with values of 25–65 g/m/s at wind speeds of 9.5–10.5 m/s at z = 1.2 m; coarse sand particles were observed to move during wind gusts; sand was also eroded at dry spots near the uprush line (about 70% moist spots and 30% dry spots). Initiation of transport with rolling particles started at wind velocities in the range of 7–8 m/s (Table 5, Appendix A). The wet intertidal beach where the armour layer is absent due to the effect of breaking waves appeared to be an important source of sand, particularly in the relatively dry zone around the HW-line in agreement with the findings of Hoonhout and de Vries (2017) at the Sand Motor mega-nourishment south of The Hague. Sarre (1988) also measured intensive sand transport over a moist beach with a very long fetch. Others (Delgado-Fernandez, 2010) found that sand transport ceased at moist beaches. Important parameters are the fetch length and the drying time near the HW-line. The fetch length at the PH-site was very long (> 500 m) at both dates with wind parallel to the beach causing rapid drying (within 3 hours) of sand around the HW-line at many spots. The sand was eroded at these relatively dry spots and then distributed over the full width of the wet beach by the wind.

6.2.2. *Dry beach with armour layer*

Sand transport was measured at the dry beach with armour layer (Fig. 2) at 20 and 40 m from the water line. Sand was eroded from between the immobile coarse materials and from upwind locations. Observed threshold wind velocities of various particle size classes are shown in Table 5 (Appendix A). The finer sand particles were mobile with threshold wind velocities in the range of 7–11 m/s. Sand and gravel particles larger than 1 mm were mostly immobile in conditions with wind velocities up to 11 m/s at z = 1 m; some movement was observed during strong wind gusts. The trapped sediment consisted of sand (no coarse gravel; no shells in LVRS-trap). Measured sand transport rates were small with values in the range of 1–7 g/m/s at wind speed of about 10 m/s at z = 1.3 m, see Fig. 9 (solid green diamonds). Three other transport measurements were done at the same (armoured) spot during the same conditions. These values are not shown in Fig. 9, as the transport rates were almost zero. It is concluded that sand transport is significantly restricted due to the presence of the armour layer; at least factor 10 compared to the other data at the same wind velocity of 10 m/s, see Fig. 9.

Sand transport was also measured on the dry south beach (1 km south of mast 2) during a minor storm event from NNE (parallel to dune). The upper layer of 5 mm was dry (moisture < 1%) and consisted of sand with some coarse gravel and shells (< 5%; no armour layer). Sand transport was intense with value of 48 g/m/s at wind of 9.5 m/s at z = 1.25 m, see Fig. 9 (red open square). This value is in good agreement with the values at beach plain The Hors at the same wind velocity and about the same sand size, which means that a minor coarse fraction (< 5%) has no substantial effect on the transport rate in windy conditions (10–14 m/s).

6.2.3. *Dune front and dune crest*

Sand transport was measured at small open spots where dune grass (marram grass) was absent. The local surface consisted of medium coarse (dry) sand and a substantial coarse fraction > 2 mm (about 20%–30%). Alternating patterns of finer and coarser areas were present; alternating patterns of dry and moist spots were also present (50%/50%). The moisture content was about 2.5% (24 h after last rainfall). Sand transport was severely restricted by the limited fetch length. The sand transport during a minor storm event was about 2 g/m/s for fetch length of about 10 m; and 13–16 g/m/s for a fetch length of about 20 m, see Fig. 9 (red open triangles).

Sand transport was also measured between the dune grass plants (4–5 plants per m^2) where medium fine, almost dry sand (moisture < 0.5%) was present. Sand transport was minor (< 0.3 g/m/s; see Fig. 9). The wind velocity between the plants was about 4–4.5 m/s at z = 0.2 m, which is about 30% lower than the values outside the dune grass area (6.6 m/s at z = 0.2 m).

Sand transport at wide open dune spots of almost dry sand without coarse materials (fetch of 30–50 m; northern area A, Fig. 11) was intense with values in the range of 75–85 g/m/s for wind speeds of about 10 m/s at z = 1.25 m from northeast, see Fig. 9 (red open diamonds). These transport rates are in good agreement with the values at beach plain The Hors at the same velocity and sand size and represent equilibrium conditions. Sand transport was substantially lower (50%–75%) at nearby spots with moist sand (moisture ≅ 4%) resulting in an irregular surface due to uneven erosion of sand.

6.3. *Predicted sand transport*

Both the single fraction and the multi-fraction methods have been used for the PH-site. The measured values at the intertidal beach (d_{50} = 0.4 mm, d_{90} = 1 mm, no gravel and shell) and at the open dune spots (d_{50} = 0.3 mm, d_{90} = 1 mm, no gravel and shell) are equilibrium values for dry sand (open circles, square, diamonds, Fig. 9). The predicted equilibrium values are also shown in Fig. 9 (red and green curves for 2 different diameters). The agreement is quite reasonable for the intertidal

beach (open circles) and the predicted values are somewhat too small (factor of 2) for the open dune spots (open diamonds). The α_w and α_{ad}-coefficients are assumed to be 1 (dry sand, long fetch). Slope effects in the dune zone were neglected as the wind was parallel to the dunes. No additional calibration was applied (default settings were used). The measured transport rates at other locations (open triangles; solid diamonds) are significantly below the predicted values of the single fraction method due to supply-limiting effects (short fetch, armour layer).

The multi-fraction was applied to the dry beach with armour layer, which is represented by 7 fractions, see Table 6 (Appendix A). The d_{50} and d_{90} of the armour layer are 0.77 mm and 5 mm. The percentage of coarse materials including shells > 2 mm is 25%. Moisture effects are neglected as the upper layer of the beach sand was dry (< 1%).

The predicted value (green dashed curve) of the multi-fraction method including the hiding-exposure factor (Equation (11); n = 0.75) is about 6 g/m/s for a wind velocity of 10 m/s. The measured values (2 data points) are in the range of 1–7 g/m/s for wind velocity of 10 m/s. Thus, the multi-fraction method yields transport values which are of the right order of magnitude. The predicted transport rates (Table 6) show that the finer fractions are transported at lower wind speeds and the coarser fractions are set in motion at higher wind speeds. At high wind speeds >15 m/s, all fractions are mobile and the transport rates of the multi-fraction method are approaching those of the single fraction method without the effect of the coarse fraction. At a wind speed of 10 m/s, the predicted values of the multi-fraction method are almost a factor of 10 smaller than those of the single fraction method (green solid curve). Thus: the measured transport rates at the armoured beach (green solid diamonds) are significantly overpredicted (factor of 10) by the single fraction method if the coarse fraction is not taken into account. The effect of the coarse fraction in the single fraction method can be simply represented by a reduction factor acting on the transport rate: $\alpha_{cf} = (1\text{-}2p_{cf}/100)^2$ with p_{cf} = percentage of coarse materials (%) as proposed by van Rijn and Strypsteen (2020). Using p_{cf} = 20% yields significantly lower transport rates, see Fig. 9 (green dotted curve), but the predicted values are still somewhat too high compared to the measured values for the armoured surface.

The multi-fraction method offers a rational approach to predict the transport of sediments for very graded beach materials including a substantial coarse fraction. The method is essential to predict the gradual development of an armour layer in a numerical model for the time evolution of the beach surface (see also Hoonhout and de Vries, 2019). This method has been extensively tested for graded sediment beds in water flow (Van Rijn, 2007), but the present results for wind flow are highly exploratory as only two data points are available for the PH-site. More field data are required under minor and major storms and more research should be done to better define the hiding-exposure coefficient.

The simpler single fraction method with inclusion of the α_{cf} -coefficient offers an attractive method with a reasonable overall accuracy; deviations are not more than a factor of 2 (green dashed, dotted curves).

7. Annual transport and loss of sand at the Prins Hendrik beach site

The modified Bagnold equation is used to calculate the annual transport of sand at the Prins Hendrik beach site with the aim to explain the annual loss of sand from this site with an armour layer. The annual loss of sand is one of the prime long-term risks in coastal management using engineered beach dunes systems. Validated estimation of these losses is therefore highly needed.

The PH-site is enclosed by the NIOZ-harbor at the south, the old traditional grass dike at the west, a traditional grass dike at the North and the Wadden Sea at the east (Fig. 10). The beach and dune are almost parallel to the dominant wind direction from southwest. The beach and spit have a layer of coarse sand, gravel and shells (about 0.3 m thick). As

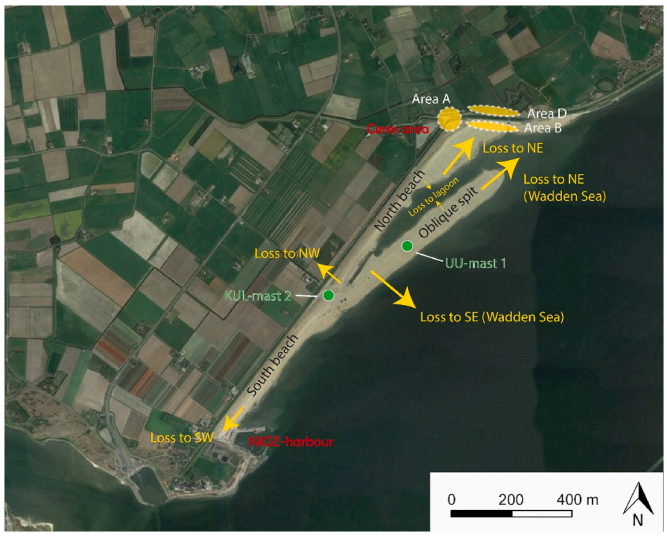

Fig. 10. Aerial view of Prins Hendrik (PH) site, Texel, The Netherlands.

there is no supply of sand across the boundaries at all, the PH- system will gradually loose sediment due to wind-induced transport and erosion. During and after construction on a timescale of 6–12 months, the fine sand fractions were removed by wind erosion resulting a top armour layer of about 10–20 mm thick. Over time, the armour layer will become slightly coarser. The loss of sand due to aeolian transport is mainly to the northeast (NE), into the Wadden Sea and to the southwest (SW), see yellow arrows of Fig. 10. No sand was observed to cross the long dune crest zone on the northwest side (NW) with dense marram grass plants during events with winds from the east to southeast. Based on visual observations and drone-based soundings, the main deposition areas are in the northern area are (Figs. 10 and 11):

- area A: northern end of the dune body where the dune crest slopes downward creating a small lee area of about 1000 m^2 with a deposition volume of about 500 m^3 (layer of 0.5 m in period June 2019–March 2020);
- area B: foot of the dike behind a long brushwood fence over a distance of about 200 m, width of about 10 m and layer thickness of about 0.3 m resulting in a volume of about 600 m^3;
- area C (in between area B and area D, see Figs. 10 and 11): in front of the fence along the maintenance road, where about 100 m^3 was removed in November 2019 and about 200 m^3 in February 2020;
- area D: at the back side of the grass dike, where about 350 m^3 was removed in February 2020 (two spots: 50x10x0.1 and 150x10x0.2).

The total deposition volume of sand in the northern areas related to wind events from southwest is about $500 + 600 + 300 + 350 \cong 1750\ m^3$ for the period June 2019 to March 2020. Adding about 150 m^3 (rough estimate) for the period March–June 2020, the total observed value for a full year is about 1900 m^3. Sand was mainly deposited in the winter period November to March. The deposited sand comes from the dry beach area with the armour layer (total area of about 400000 m^2). Assuming a layer thickness of about 10–20 mm, the total volume of the armour layer is about 4000–8000 m^3. Initially, the composition of the top layer was about 75% of sand and 25% of coarse materials. Thus, about 3000–6000 m^3 of sand has been eroded to develop the armour layer of mainly coarse materials > 2 mm during and shortly after the construction of the site. The deposition volumes from Areas C and D are regularly removed by a shovel and brought back to the beach zone. During the observation period between June 2019 and March 2020, the site experienced one major storm event from the southwest in February 2020 with wind velocities up to 20 m/s (BF9). The beach survey in March 2020 did not show any major disruption of the armour layer and

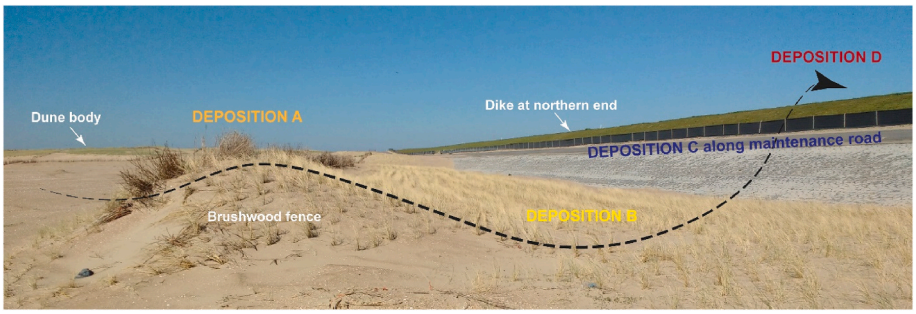

Fig. 11. Deposition areas near northern end of Prins Hendrik (PH) site, Texel.

the deposition of sand in the northern area was not excessive (< 500 m^3). These are all indications that the armour layer is not much affected by a major storm event. Coarse gravel and shells may have been mobilized, but the transport rates of coarse grains were most like relatively small.

The measured deposition volume in the northern area has been used to check the annual loss of sand predicted by the modified Bagnold-method in the period January to December of the year 2019 (first year after completion of the dredging and construction works). Annual wind data at the PH site in 2019 is not available and will therefore be taken from the weather station The Kooy near Den Helder (about 10 km from the site). However, the wind velocities at the PH-site on Texel are slightly different from those at The Kooy. This was studied by comparing the wind data of mast 1 and mast 2 and the wind data of The Kooy in the period 12 March to April 6, 2020 (field survey period). The wind data at The Kooy are measured at a height of 10 m and are converted to a value at 2 m using a logarithmic velocity profile with roughness $k_s = 0.03$ m. Based on this analysis, it is found that the wind velocity defined at 2 m above the surface at the PH-site is significantly higher than at the land station The Kooy, as follows: 25% higher for the sector 0-60°, 40% higher for the sector 60°-180°; 10% higher for the sector 180°-240° and 10% lower for the sector 240°-330° in the lee of the new dune. Using these results, the annual wind climate of The Kooy is modified to obtain a reliable annual wind climate for the PH-site. The fetch at the beach is short for the directions 240° to 300° when the beach is in the lee of the new dune, which is taken into account using the α_{ad}-coefficient. The α_{ad}-coefficient is determined by using: $\alpha_{ad} = 0.5b/[(0.1+\cos\alpha_w)L_{ad}]$ with b = beach width, α_w = angle between wind vector and shore normal, L_{ad} = distance to obtain equilibrium transport (= 100 m). The α_{ad}-values are in the range of 0.3–1. The predicted transport vector values are decomposed in 4 components: parallel to the beach in northeast (NE) and southwest (SW) and normal to the beach in northwest (NW) and southeast (SE). The coastline angle is 40° to the north. The predicted annual transport rates are shown in Table 7 for three cases. Case A: only dry sand without coarse materials. Case B: dry sand with a coarse fraction of gravel and shells which is represented by $\alpha_{cf} = (1\text{-}2p_{cf}/100)^2$ in Equation (4) with p_{cf} = percentage coarse fraction > 2 mm as proposed by van Rijn and Strypsteen (2020). Case C: moist sand with coarse fraction.

The rain in mm per hour from station De Kooy is converted to a moisture content (w_{20}) of the top layer with thickness of 20 mm. The moisture of the intertidal beach varies from the LW-line (about 12%) to the HW-line (about 4%), which is represented by a constant value of 8%. The effect of the moisture content on the threshold shear velocity (Equation (5)) is included by using $\alpha_w = 1 + 0.1w_{20}$ as proposed by van Rijn and Strypsteen (2020). Furthermore, the drying of the sand surface after the end of a rainfall period is included by assuming a short drying time of 6 h in June (summer) and long drying time of 24 h in December (winter) and a linear decrease of the moisture coefficient to 2% during the drying time. Table 7 under Case C shows two numbers: the first with inclusion of the drying effect (smaller transport) and the second without the drying effect.

The transport rates of Case A for dry sand without coarse fraction are highest and the transport rates of Case C for moist sand with the coarse fraction and the drying effect included are smallest. The transport at the dry beach to the northeast (NE) is highest with a value of about 35 m^3/m/year for Case A as winds are from the southwest are most frequent (750 h per year with wind velocity > 10 m/s). The transport to the southeast (SE) is smallest because winds from west to north are less frequent (200 h with wind velocity > 10 m/s). During these latter conditions, the dry beach is in the lee of the new dune resulting in a reduction of the effective wind velocity and a relatively short fetch at the beach. As a result, the transport to the southeast (SE) is relatively small with a value of 3.6 m^3/m/year for Case A and 1 m^3/m/year for Case C.

The total loss of sand is caused by transport to the northeast, to the southwest and to the southeast and is computed as:

$$Q_{sand,ne} = b_{intertidal}\, q_{s,intertidal,ne} + b_{beach}\, q_{s,beach,ne} + b_{spit}\, q_{s,spit,ne} + b_{dune}\, q_{s,dune,ne}$$
$$Q_{sand,sw} = b_{intertidal}\, q_{s,intertidal,sw} + b_{beach}\, q_{s,beach,sw} + b_{dune}\, q_{s,dune,sw}$$
$$Q_{sand,se} = L_{beach}\, q_{s,intertidal,se}$$

The width (b) of the intertidal zone between the HW and LW lines is about 20 m; the width of the dry beach is set to 150 m for the north beach and to 60 m for the south beach. The width of the spit is set to 150 m. The width of the dune zone without marram grass is about 10 m. The alongshore beach length (L) is about 2 500 m. The loss of sand from the armoured beach zone to the northwest is not shown as this value is small (<1 m^3/m/year; only 30 h with wind from sector east to south and wind speeds > 10 m/s). Sand carried to northwest is trapped in the dune zone with marram grass plants and is not a real loss as it contributes to dune growth. Almost no sand was observed to pass the dune crest zone with dense marram grass plants. There may also be a small (internal) loss to the Lagoon.

The total transport and loss of sand to the northeast is predicted to be: $Q_{sand,ne}$ = 11340 m^3/year for Case A, 4480 m^3/year for Case B and 3550 m^3/year for Case C, see Table 7. This latter value is the most realistic loss of sand to the northeast including all effects. About 50% (1775 m^3/year) of the predicted value of 3550 m^3/year to northeast comes from the north beach/dune zone and is deposited in the northern areas (A to D) and is in good agreement with the observed deposition of about 1750–1900 m^3/year in the northern area in the period June 2019–June 2020. The other part (1775 m^3/m/year to northeast) comes from the spit and is deposited into the Wadden sea at the end of the spit, see Fig. 10. The total transport and loss of sand to southwest is about 225 m^3/year for Case C. The transport and loss of sand to the southeast (to the Wadden Sea) is about 3000 m^3/year for Case C. This latter value is quite substantial which is caused by the long beach length of about 2500 m. The total predicted loss of sand to Wadden Sea is about 1775 + 3000 ≅ 4775 m^3/year for Case C. The total loss of sand due to aeolian processes is about 6800 m^3/year for the most realistic Case C. Taking the small loss of sand to the Lagoon into account, the overall loss of sand will be about 7000–8000 m^3/year. This is equivalent with an erosion layer of sand of about 17–20 mm assuming a total area at the PH-site of 400000

m^2.

This example shows that the aeolian loss of sand from an artificial beach can be significantly reduced (factor 3 to 4; total loss for Case A ≅ 30000 m^3/year) by the placement of a layer of coarse sediment and shells on the beach surface, based on model predictions with the modified Bagnold model which was to some extent verified using measured transport rates at the armoured beach. More field data under major storms are required for more firm conclusions. It is logic to assume that the loss of sand is highest in the first year and will be smaller in later years, as the armouring effect of the coarse layer may improve slightly. The annual loss of sand from the beach and dune zones in the coming years is estimated to be in the range of 2500–5000 m^3/year.

Finally, it is noted that these exploratory results are a first step to estimate the loss of sand due to wind erosion at a rather complex site with an armour layer at the dry beach. In future, the more detailed 2D Aeolis model (Hoonhout and de Vries, 2019) will be applied to this site. However, it is not a priori certain that this will lead to more accurate estimates as many model coefficients may have to be calibrated.

8. Summary and conclusions

Detailed field studies on aeolian sand transport in conditions with sand, gravel, shells and moving and stationary bed forms have been conducted at two beach sites at Texel, the Netherlands: a wide and exposed sandy beach plain (The Hors) with an enormous fetch length (> 500 m) and a new sheltered dune-beach-spit system with coarse sediments (Prins Hendrik site). At this latter site, the supply and transport of sediment is limited by the presence of non-erodible coarse grains at the beach surface. Mobile and immobile bed forms are characteristic features at both sites. Knowledge of bed roughness under varying wind conditions is of utmost importance for engineering computations. This was studied by comparing overall shear velocity derived from measured wind velocity profile data to predicted values at both sites.

Various sand transport traps have been used to measure aeolian sand transport as function of wind velocity: the traps of Bagnold and Sarre at the beach plain site The Hors and the streamer-type trap of LVRS at the PH-site. A special trap for creep transport has been used at the beach plain The Hors to determine the contribution of creep-type transport to the overall transport. Transport measurements at the more complex PH-site have been done at the wet beach, dry beach, dune foot, dune front and dune crest during various minor storm events.

Sediment transport predictions have been made using the single and multi-fraction methods based on the modified Bagnold transport equation with default settings. Using the single-fraction method, the sand particles of the beach surface are represented by the d_{50} and d_{90} of the sand mixture. Using the multi-fraction method, the sand mixture is represented by multiple fractions, each with its own mean diameter and a hiding-exposure factor to deal with hiding-exposure effects, as the finer particles are hiding between the coarser grains and are more difficult to set into motion. The prediction methods have been used to estimate the annual loss of sand from the new PH-site.

The main findings of the studies are, as follows:

1. The roughness values of mobile bed forms at the sandy beach plain The Hors and stationary bed forms at the PH-site are up to 150 mm; the high bed roughness values are mainly related to the form roughness of the bed forms; measured shear velocity values are higher than the predicted dynamic grain-related shear velocity used in the transport model.
2. The creep-quotient (ratio of creep transport and saltation transport) is dependent on shear velocities and is not the constant (1/3) as proposed by Bagnold. The quotient is around 0.5 for low shear velocities and drops to 0.2 for higher shear velocities. The transport rates of dry sand measured at the beach plain The Hors show a clear increase for increasing shear velocity (approximately power 3) and can be reasonably well represented by the modified Bagnold equation based on predicted grain-related shear velocities.
3. The measured sand transport rates at the sandy parts (dunes, south beach) of the Prins Hendrik site are very comparable to the transport rates at the beach plain The Hors and are slightly underpredicted by the modified Bagnold equation.
4. The transport rates in the dry beach zone and in the dune front/crest zone of the PH-site are severely restricted (factor 10) by the armour layer of coarse grains; the restricted transport in the dry beach zone with armoured top layer can be reasonably well represented by the Bagnold model using a multi-fraction approach with hiding-exposure factor.
5. The new beach dune site Prins Hendrik suffers from erosion, as there is no supply of sand from the upwind boundaries; the annual deposition of sand in the northern area in the first year after construction was observed to be about 1900 m^3/year; the predicted loss of sand in the northern area based on the modified Bagnold equation is about 1775 m^3/year including the effects of coarse materials and moisture due to rainfall.
6. The aeolian loss of sand from an artificial beach can be significantly reduced (factor 3 to 4) by the placement of a layer of coarse sand, gravel and shells on the beach surface; this is based on model predictions with the modified Bagnold-model; measured transports at the armoured beach were correctly represented by the model.

Author Statement

Glenn Strypsteen: Conceptualization, Methodology, Software, Resources, Validation, Visualization, Investigation, Formal analysis, Data curation, Writing- Original Draft, Writing – Review & Editing.

Leo van Rijn: Conceptualization, Methodology, Investigation, Formal analysis, Data curation, Writing- Original Draft, Writing – Review & Editing.

Max Hoogland: Investigation, Formal analysis, Data curation.

Pieter Rauwoens: Resources, Supervision, Project administration, Writing – Review & Editing, Conceptualization.

Jan Fordeyn: Resources, Project administration, Writing – Review & Editing.

Marc Hijma: Writing- Original Draft, Writing – Review & Editing, Investigation, Formal analysis, Data curation, Resources.

Quirijn Lodder: Writing- Original Draft, Writing – Review & Editing, Investigation, Formal analysis, Data curation, Resources.

Declaration of competing interest

The authors declare that they have no known competing financial interests or personal relationships that could have appeared to influence the work reported in this paper.

Acknowledgements

The Dutch water board Hoogheemraadschap Hollands Noorderkwartier and the Belgian marine contractor Jan De Nul N.V. are gratefully acknowledged for providing funds and logistics for this study. We thank the support of VLIZ (Flanders Marine Institute) for the use of their aeolian research infrastructure.

Appendix A. Tables

Table 1
Summary of wind velocity, shear velocity and roughness for the beach plain of The Hors, Texel, The Netherlands.

Site	Measured u_* (m/s)	$U_{1.3m}$ (m/s)	U_{2m} (m/s)	Measured k_s (cm)	Predicted k_s (cm)
The Hors beach plain (d_{50} = 0.23 mm)	0.19 (0.15–0.20)	4.30 (3.31–4.41)	4.51 (3.47–4.63)	0.57	0
	0.22 (0.20–0.25)	5.02 (4.64–5.80)	5.26 (4.86–6.07)	0.36 (0.20–0.52)	0
	0.28 (0.25–0.30)	5.63 (5.09–6.11)	5.93 (5.36–6.43)	1.13 (0.70–1.57)	0
	0.32 (0.30–0.35)	6.52 (6.16–7.19)	6.86 (6.49–7.57)	1.05 (0.67–1.43)	0.41
	0.38 (0.35–0.40)	7.25 (6.66–7.61)	7.66 (7.04–8.04)	1.93 (1.44–2.42)	0.45
	0.43 (0.40–0.45)	7.89 (7.33–8.24)	8.35 (7.76–8.73)	2.56 (1.90–3.22)	0.53
	0.48 (0.45–0.50)	8.57 (8.00–8.89)	9.09 (8.48–9.43)	3.19 (2.09–4.28)	0.63
	0.52 (0.50–0.55)	8.66 (8.35–9.18)	9.21 (8.89–9.78)	4.90 (3.92–5.89)	0.62
	0.58 (0.55–0.60)	9.56 (9.13–9.96)	10.18 (9.72–10.60)	5.11 (3.64–6.58)	0.76
	0.62 (0.60–0.65)	9.79 (9.43–10.22)	10.46 (10.08–10.92)	7.25 (4.37–10.14)	0.79
	0.72 (0.70–0.75)	12.20 (11.86–12.71)	12.97 (12.61–13.51)	4.45	1.18
	0.85 (0.80–0.85)	13.05 (12.35–13.12)	13.96 (13.21–14.04)	8.11	1.36

Table 2
Wind velocity, shear velocity and roughness of The Hors beach plain and PH-beach, Texel, The Netherlands.

Site	U_{1m} (m/s)	u_* (m/s)	k_s (mm)	Bed forms
The Hors beach plain	3.5–7	0.2–0.4	2–50	plain and small ripples
(d_{50} = 0.23 mm)	7–9	0.4–0.5	10–50	small migrating ripples height 20 mm; length 0.2 m
	9–11	0.5–0.6	50–100	migrating mega ripples height = 50 mm; length = 0.5 m
	11–14.5	0.6–0.8	50–100	migrating mega ripples height = 50 mm; length = 0.5 m
PH-beachMarch 27, 2020	8–11	0.48–0.62 (mast 1)	70–150	undulations height 100–250 mm; length 1–3 m
(armour layer; d_{50} = 0.5–1 mm)	7–10	0.42–0.57 (mast 2)	20–50	undulations height 50–150 mm; length 1–3 m
	7–9	0.37–0.56 (short mast)	10–50	undulations height 50–150 mm; length 1–3 m

Table 3
Summary of transport data for beach plain of The Hors (d_{50} = 0.23 mm; dry sand; fetch > 500 m).

Measured u_* (m/s)	$U_{1.3m}$ (m/s)	U_{2m} (m/s)	Measured $Q_{s,Bagnold}$ (g/m/s)	Measured $Q_{s,Creep}$ (g/m/s)	Measured $Q_{s,Sarre}$ (g/m/s)
0.19 (0.15–0.20)	4.30 (3.31–4.41)	4.51 (3.47–4.63)	0.39	/	/
0.22 (0.20–0.25)	5.02 (4.64–5.80)	5.26 (4.86–6.07)	0.93	0.48	1.51
0.28 (0.25–0.30)	5.63 (5.09–6.11)	5.93 (5.36–6.43)	3.74	1.55	3.88
0.32 (0.30–0.35)	6.52 (6.16–7.19)	6.86 (6.49–7.57)	7.07	3.03	8.88
0.38 (0.35–0.40)	7.25 (6.66–7.61)	7.66 (7.04–8.04)	25.37	5.63	18.76
0.43 (0.40–0.45)	7.89 (7.33–8.24)	8.35 (7.76–8.73)	31.74	4.82	18.46
0.48 (0.45–0.50)	8.57 (8.00–8.89)	9.09 (8.48–9.43)	49.04	6.81	36.89
0.52 (0.50–0.55)	8.66 (8.35–9.18)	9.21 (8.89–9.78)	22.39	5.76	22.62
0.58 (0.55–0.60)	9.56 (9.13–9.96)	10.18 (9.72–10.60)	22.80	5.28	30.35
0.62 (0.60–0.65)	9.79 (9.43–10.22)	10.46 (10.08–10.92)	65.41	5.33	41.80
0.72 (0.70–0.75)	12.20 (11.86–12.71)	12.97 (12.61–13.51)	/	/	126.89
0.85 (0.80–0.85)	13.05 (12.35–13.12)	13.96 (13.21–14.04)	144.93	/	/

Table 4
Summary of transport data for PH beach site, Texel, The Netherlands

Date, time and weather	Beach		Moisture (%)			Wind conditions		Sand transport q (g/m/s)
	d_{50};d_{90} (mm) p_{coarse} (%)	Description	upper 5 mm	upper 20 mm	p_m (%)	$U_{1.3m}$ and u_* (m/s)	Upwind fetch length (m)	
March 12, 2020; 10h30; Te = 9 °C; BF7	0.45; 3; >30	mid dry beach; bed undulations; armour layer	nm	1.7	70	10; 0.59	75–100	7
12 March 13h05; Te = 9 °C; BF7	0.45; 3; >30	mid dry beach; bed undulations; armour layer	nm	2	70	10; 0.59	75–100	1
12 March; 13h35 Te = 9 °C; BF7	0.4; 1; 2–20	wet beach; flat, smooth	11	11	70	10.5; 0.6	300	65
12 March; 14h40; Te = 9 °C; BF7	0.4; 1; 2–20	wet beach; flat, smooth	<8	8	70	9.5; 0.48	300	27
21 March; 12h15; Te = 7 °C; BF5/6	0.3; 0.9; <5	dune front; flat; smooth	nm	2.5	50	9; 0.53	10	2.2
21 March; 12h45; Te = 7 °C; BF5/6	0.3; 0.9; <5	dune front; flat; smooth	nm	2.5	50	9.3; 0.61	20	16.2
21 March; 13h05; Te = 7 °C; BF5/6	0.3; 0.9; <5	dune front; flat; smooth	nm	2.5	50	9.3; 0.61	20	13.5
21 March; 13h20; Te = 7 °C; BF5/6	0.3; 0.9; <1	dune front between grass plants	<0.5	<0.5	0	8.8; 0.85	5	0.3
27 March; 13h40; Te = 9 °C; BF6	0.4; 1; 10	wet beach; flat, smooth	<12	12	70	9.6; 0.62	100	35
27 March; 13h57; Te = 9 °C; BF6	0.4; 1; 10	wet beach; flat, smooth	<12	12	70	9.6; 0.62	100	25
27 March; 14h20; Te = 9 °C; BF6	0.3; 0.9; >30	dune foot; undulations; armour layer	<0.5	<0.5	0	9; 0.59	100	0.35
29 March; 13h10; Te = 6 °C; BF6/7	0.26; 0.5; <1	dune crest; smooth sloping surface	<0.5	<0.5	0	10.5; 0.73	30	88
29 March; 13h10; Te = 6 °C; BF6/7	0.26; 0.5; <1	dune crest; smooth sloping surface	<0.5	<0.5	0	10.7; 0.83	30	78
29 March; 14h35; Te = 6 °C; BF6/7	0.26; 0.5; <1	dune crest; smooth sloping surface	<0.5	<0.5	0	9.8; 0.8	30	68
29 March; 14h05; Te = 6 °C; BF6/7	0.26; 0.5; <1	dune crest; irregular sloping surface	nm	4	50	9.5; 0.64	50	25
29 March NIOZ; 15h10; Te = 6 °C; BF6/7	0.27; 0.5; <1	dry beach; small undulations	<1	2	0	9.5; 0.64	30	48

BF = Beaufort wind scale; p_m = percentage of beach surface with moist appearance at measurement location; nm = not measured; p_{coarse} = coarse fraction of grave and shells > 2 mm.

Table 5
Threshold wind speeds of dry sand and gravel material (initiation of motion; $\alpha_{th} = 0.1$), PH beach site, Texel.

Sediment (mm)	Threshold shear velocity (based on Bagnold-model) (m/s)	Threshold wind velocity at 1 m above surface (m/s)		Threshold wind velocity at 10 m above surface based on Bagnold-model (m/s)
		Based on Bagnold	Observed (12 March-22 April 2020)	
0.2	0.21	5.8	6	7.0 (BF4)
0.4	0.29	7.7	7.5	9.4 (BF5)
0.6	0.36	9.1	9	11.2 (BF6)
0.8	0.42	10.2	10	12.6 (BF6)
1	0.47	11.2	immobile	13.9 (BF7)
2	0.66	14.7	immobile	18.5 (BF8)
4	0.93	19.1	immobile	24.5 (BF9)
6	1.14	22.3	immobile	28.9 (BF10)
10	1.47	26.9	immobile	35.4 (BF12)

Table 6
Predicted sand transport of single and multi-fraction methods for dry beach; PH beach site, Texel

Wind speed at z = 1.3 m (m/s)	Sediment transport single fraction d_{50} = 0.77 mm (g/m/s)	Sediment transport based on multi fraction method (g/m/s)							
		0.2 mm 0.1–0.3 5%	0.4 mm 0.3–0.5 10%	0.6 mm 0.5–0.7 15%	0.85 mm 0.7–1 25%	1.5 mm 1–2 20%	3 mm 2–4 15%	7 mm 4–10 5%	Total
9.5	3.1	0	0	0.29	0.87	0	0	0	1.16
10	8.0	0	0.2	1.75	3.75	0	0	0	5.7
10.5	13.6	0	1.14	3.41	7.05	0	0	0	11.6
11	20.0	0.093	2.17	5.32	10.84	1.18	0	0	19.6
11.5	26.2	0.45	3.17	7.17	14.5	5.11	0	0	30.4
12	32.4	0.83	4.17	9.0	18.2	9.0	0	0	41.2
13	47.0	1.65	6.55	13.4	26.8	18.2	0	0	66.6
14	65.2	2.7	9.5	18.8	37.5	29.6	0	0	98.1
15	87.4	4.0	13.1	25.4	50.6	43.5	11.3	0	147.9

Table 7
Predicted annual transport at PH-site with beach length of 2 500 m, Texel.

Case	Annual sand transport parallel to beach in northeast, southwest and southeast direction (m^3/m/year)			Total loss of sand (m^3/year)
	Intertidal zone d_{50} = 0.4 mm d_{90} = 1 mm coarse > 2 mm = 10%	Armoured beach zone d_{50} = 0.77 mm d_{90} = 3 mm coarse > 2 mm = 20%	Dune zone (no plants) Total d_{50} = 0.295 mm d_{90} = 1 mm coarse> 2 mm = 5%	
A. Dry sand (no coarse fraction)	NE-transport = 30 SW-transport = 6 SE-transport = 3.5	NE-transport = 35 SW-transport = 8 SE-transport = 3.6	NE-transport = 24 SW-transport = 5 SE-transport = 3.5	NE 11340 SW 650 SE 8 750
B. Dry sand with inclusion coarse fraction	NE-transport = 19 SW-transport = 4 SE-transport = 2.2	NE-transport = 13 SW-transport = 3 SE-transport = 1.3	NE-transport = 20 SW-transport = 4 SE-transport = 2.8	NE 4 480 SW 300 SE 5 500
C. Sand with inclusion coarse fraction and moisture (no transport on rainy days + 1 day drying)	NE-transport = 10-14 SW-transport = 1.7–2.6 SE-transport = 1–1.5	NE-transport = 10-11 SW-transport = 2.4–2.6 SE-transport = 1–1.1	NE-transport = 16-17 SW-transport = 2.4–2.6 SE-transport = 1–1.1	NE 3 550 SW 225 SE 3 000

References

Al Khalaf, A., 1986. Specification and Calibration of Bagnold's Model for Sand Transport: Urayq Al Buldan, Dune Field, Central Saudi Arabia. Doctoral Thesis. Indiana University, Bloomfield, USA.

Bagnold, R.A., 1937. The transport of sand by wind. Geogr. J. 89, 409–438.

Bagnold, R.A., 1938. The measurement of sand storms. Proceedings of the Royal Society of London Series A 167, 282–291.

Bagnold, R.A., 1941, 1954. The Physics of Blown Sand and Desert Dunes. Methuen, New York.

Bauer, B.O., Sherman, D.J., Wolcott, J.F., 1992. Sources of uncertainty in shear stress and roughness length estimates derived from velocity profiles. Prof. Geogr. 44 (4), 453–464. https://doi.org/10.1111/j.0033-0124.1992.00453.x.

Carter, R.W.G., 1976. Formation, maintenance and geomorphological significance of an aeolian shell pavement. SEPM Journal of Sedimentary Research 46 (2), 418–429. https://doi.org/10.1306/212f6f8c-2b24-11d7-8648000102c1865d.

Carter, R.W.G., Rihan, C.L., 1978. Shell and pebble pavements on beaches: examples from the North coast of Ireland, 5, pp. 365–374. May 1973.

Chepil, W.S., Woodruff, N.P., 1963. The physics of wind erosion and its control. Adv. Agron. 15, 211–302. https://doi.org/10.1017/CBO9781107415324.004.

Delgado-Fernandez, I., 2010. A review of the application of the fetch effect to modeling sand supply to coastal foredunes. Aeolian Research 2, 61–67.

De Vries, S., van Thiel de Vries, J.S.M., van Rijn, L.C., Arens, S.M., Ranasinghe, R., 2014. Aeolian sediment transport in supply limited situations. Aeolian Research 12, 75–85. https://doi.org/10.1016/j.aeolia.2013.11.005. October 2015.

Egiazaroff, I.V., 1965. Calculation of nonuniform sediment concentrations. Journal of Hydraulics Division, ASCE 91 (4), 225–247.

Ellis, J.T., Li, B., Farrell, E.J., Sherman, D.J., 2009. Protocols for characterizing aeolian mass-flux profiles. Aeolian Research 1 (1–2), 19–26. https://doi.org/10.1016/j.aeolia.2009.02.001.

Field, J.P., Pelletier, J.D., 2018. Controls on the aerodynamic roughness length and the grain-size dependence of aeolian sediment transport. Earth Surf. Process. Landforms 43 (12), 2616–2626. https://doi.org/10.1002/esp.4420.

Gilette, D.A., Stockton, P., 1989. The effect of non-erodible particles on wind erosion of erodible surfaces. J. Geophys. Res. 94 (12), 885–893.

Gillies, J.A., Nickling, W.G., King, J., 2006. Aeolian sediment transport through large patches of roughness in the atmospheric inertial sublayer. J. Geophys. Res.: Earth Surface 111 (2), 1–13. https://doi.org/10.1029/2005JF000434.

Goossens, D., Offer, Z.Y., 2000. Wind tunnel and field calibration of five aeolian dust samplers. Atmos. Environ. 34 (7), 1043–1057. https://doi.org/10.1016/S1352-2310(99)00376-3.

Han, Q., Qu, J., Liao, K., Zhu, S., Zhang, K., Zu, R., Niu, Q., 2011. A wind tunnel study of aeolian sand transport on a wetted sand surface using sands from tropical humid coastal southern China. Environmental Earth Sciences 64 (5), 1375–1385. https://doi.org/10.1007/s12665-011-0962-7.

Hijma, M.P., Lodder, Q., 2001. An Evaluation of Aeolian Sand Transport Models Using Four Different Sand Traps at the Hors, Texel. MSc Thesis. Department of Physical Geography, University of Utrecht, The Netherlands. https://dspace.library.uu.nl/handle/1874/32882.

Hoonhout, B., de Vries, S., 2017. Field measurements on spatial variations in aeolian sediment availability at the Sand Motor mega nourishment. Aeolian Research 24, 93–104. https://doi.org/10.1016/j.aeolia.2016.12.003.

Hoonhout, B., de Vries, S., 2019. Simulating spatiotemporal aeolian sediment supply at a mega nourishment. Coast Eng. 145, 21–35. https://doi.org/10.1016/j.coastaleng.2018.12.007. March 2018.

Hoonhout, B.M., de Vries, S., 2016. A process-based model for aeolian sediment transport and spatiotemporal varying sediment availability. J. Geophys. Res.: Earth Surface 121 (8), 1555–1575. https://doi.org/10.1002/2015JF003692.

Lyles, L., Schrandt, R.L., Schmeidler, N.F., 1974. How aerodynamic roughness elements control sand movement. Trans. ASAE (Am. Soc. Agric. Eng.) 17 (1), 134–139. https://doi.org/10.13031/2013.36805.

McKenna Neuman, C., Li, B., Nash, D., 2012. Micro-topographic analysis of shell pavements formed by aeolian transport in a wind tunnel simulation. J. Geophys. Res.: Earth Surface 117 (4), 1–16. https://doi.org/10.1029/2012JF002381.

Nickling, W.G., McKenna, N.C., 1995. Development of deflation lag surfaces. Sedimentology 42, 403–414.

Nikuradse, J., 1933. Stromungsgesetz in Rauhren Rohren, vDI Forschungshefte 361 (English Translation: Laws of Flow in Rough Pipes). Tech. Rep. NACA Technical Memorandum, 1292.

Pelletier, J.D., Field, J.P., 2016. Predicting the roughness length of turbulent flows over landscapes with multi-scale microtopography. Earth Surface Dynamics 4 (2), 391–405. https://doi.org/10.5194/esurf-4-391-2016.

Sarre, R.D., 1988. Evaluation of aeolian sand transport equations using intertidal zone measurements. Saunton Sands, England, Sedimentology 35, 671–679.

Shao, Y., Lu, H., 2000. A simple expression for wind erosion threshold friction velocity. J. Geophys. Res. 105, 22437–22443.

Sherman, D.J., 1990. A method for measuring Aeolian sediment transport rates. Proceedings of the Symposium on Coastal Sand Dunes 37–47.

Sherman, D.J., Hotta, S., 1990. Aeolian sediment transport: theory and measurement. In: Nordstrom, K.F., Psuty, N.P., Carter, B. (Eds.), Coastal Dunes, Form and Process. Chester, Wiley and Sonds Ltd., pp. 17–37

Sherman, D.J., Jackson, D.W.T., Namikas, S.L., Wang, J., 1998. Wind-blown sand on beaches: an evaluation of models. Geomorphology 22 (2), 113–133. https://doi.org/10.1016/S0169-555X(97)00062-7.

Sherman, D.J., Li, B., Ellis, J.T., Farrell, E.J., Maia, L.P., Granja, H., 2013. Recalibrating aeolian sand transport models. Earth Surf. Process. Landforms 38 (2), 169–178. https://doi.org/10.1002/esp.3310.

Sherman, D., Swann, C., Barron, D., 2014. A high-efficiency, low-cost aeolian sand trap. Aeolian Research 13, 31–34.

Strypsteen, G., 2019. Monitoring and Modeling Aeolian Sand Transport at the Belgian Coast (Doctoral Thesis). KU Leuven, Belgium.

Tan, L., Zhang, W., Qu, J., Zhang, K., An, Z., Wang, X., 2013. Aeolian sand transport over gobi with different gravel coverages under limited sand supply: a mobile wind tunnel investigation. Aeolian Research 11, 67–74. https://doi.org/10.1016/j.aeolia.2013.10.003.

Van Der Wal, D., 1998. The impact of grain size distribution of nourishment sand on aeolian sand transport. J. Coast Res. 14, 620–631.

Van Rijn, L.C., 2007. Unified view of sediment transport by currents and waves. III: graded beds. J. Hydraul. Eng. 133 (7), 761–775.

Van Rijn, L.C., 2020. Aeolian Sand Transport and Erosion at the Prins Hendrik Site. Texel. www.leovanrijn-sediment.com.

Van Rijn, L.C., Strypsteen, G., 2020. A fully predictive model for aeolian sand transport. Coast Eng. 156 (October 2019), 103600. https://doi.org/10.1016/j.coastaleng.2019.103600.

Wang, Z.T., Zheng, X.J., 2004. Theoretical prediction of creep flux in aeolian sand transport. Powder Technol. 139 (2), 123–128. https://doi.org/10.1016/j.powtec.2003.11.001.